Enhanced scattering from a planar waveguide structure with a slightly rough boundary

Zhi Liang Wang,* Hisanao Ogura, and Nobuyuki Takahashi
Department of Electronics, Kyoto University, Yoshida, Kyoto 606, Japan
(Received 30 January 1995)

The scattering problem of an incident wave from a waveguide structure with a slightly rough surface is studied. The waveguide structure is considered to be a dielectric film deposited on a planar, perfectly conducting metal surface, and the top surface of the film is assumed to be a randomly rough surface. The stochastic scattered wave fields are represented in terms of orthogonal functionals with the Wiener coefficients. These coefficients are determined by applying the approximated boundary conditions expanded up to the third order of the random surface function. The analytical expressions for the coefficients of the first three terms are obtained rigorously up to the second order of the surface roughness so as to satisfy the reciprocity. It can be easily shown that our results are the same as those obtained by perturbation theory if we expand them in powers of the surface roughness. However, we have the so-called mass operator in the denominator of the coefficients, which can be used to determine the perturbed propagation constants of the guided waves in the presence of a rough surface and remove the divergence difficulty in the common perturbation theory. The numerical calculations show that there are some well-pronounced satellite peaks in the incoherent scattering distribution, in addition to the enhanced backscattering peak, when the waveguide structure can support two or more than two guided modes. This is caused by the interference of two double-scattering processes and is attributed to the existence of the guided waves in the scattering structure.

I. INTRODUCTION

Scattering of waves from a random rough surface is a problem not only of theoretical interest but also of practical importance, and at the same time it is a very common physical phenomenon.[1–4] The problem can evidently be divided into two groups.[2] The first group is related to interactions of the waves in free spaces or half spaces with rough surfaces, for instance, the scattering of radio waves from irregular ground or sea surfaces, the wave diffraction from a rough body, and the excitation of surface plasmons in random metal surfaces. Common to all these situations is that the wave field interacts with only a finite portion of the surface, namely, a single act of scattering from the rough surface. Afterwards, the scattered waves travel in free space and never interact again with the boundary irregularities. For this reason, only slight distortions of the wave field can be produced if the perturbations of the boundary irregularity are small enough, and as a result, even the first Born approximation of perturbation theory gives satisfactory solutions.

The second group is related to interactions of waves with the rough surfaces in a waveguide structure, and it can be further divided into two kinds of problems according to the location of the excitation source, that is, the interior problem in which the source is located inside the waveguide, and the exterior problem in which a wave incident on the rough surface from outside the waveguide. Due to the existence of the guided modes in such structures, the waves can interact with the rough irregularities again and again (coherent multiple scattering), and it leads to some different or new effects absent in the case of free spaces or half spaces. For example, there is a stronger enhanced backscattering peak when the structure can support the guided modes and the additional satellite peaks appear when the structure can support two or more guided modes.

By using the stochastic functional approach, we have successfully studied the scattering problems of guided waves in a planar waveguide and an optical fiber with a slightly rough boundary,[5,6] which obviously belong to the interior problem. The approach was first introduced in the theory of propagation in random media by one of the authors,[7–9] and has been used successfully to develop the scattering theory of a plane scalar or electromagnetic wave from various planar,[10–15] cylindrical,[16–18] and spherical[19] random rough surfaces with small roughness. In these works, the scattered wave field is regarded as a stochastic functional of the random surface that can be represented in the form of the Wiener-Hermite expansion[21,22] in the case of a Gaussian random surface, and a group-theoretic consideration is made to determine the form of a stochastic wave field based on the statistical homogeneity of the random surface, which is analogous to the Floquet theorem for a periodic boundary. A set of hierarchical equations for the expansion coefficients is obtained from the boundary conditions and can be solved by making use of the recurrence relations and the orthogonality of the Wiener-Hermite functionals. Various statistical characteristics of the scattered waves, such as coherent and incoherent fields, their differential cross section (the second-order moments), and angular distribution etc., can be easily calculated. More importantly, it has been shown that the so-called divergence difficulty in the common perturbation theory, which is due to the multiple scattering in the direction close to the planar random surface, is automatically removed in our approach owing to the "stochastic Floquet theorem" and

0163-1829/95/52(8)/6027(15)/$06.00

the stochastic functional calculus.[12] This means that the stochastic functional approach is good enough for treating the multiple-scattering effects, and hence can be applied to the scattering problems from rough surfaces related to a waveguide structure. In fact, we have also considered a similar problem in a previous paper,[13] in which the excitation of surface plasmons (modes) in a Ag film with a rough surface was studied for the incident plane wave from outside.

In this paper we extend the stochastic functional approach to the scattering problem of an incident wave from a planar waveguide with a slightly rough surface. The waveguide structure is considered to be a dielectric film deposited on a planar, perfectly conducting metal surface, and the top surface of the film is assumed to be a randomly rough surface, as shown in Fig. 1. We note that the same problem has been studied recently by using the perturbation theory.[23–25] The perturbation theory is a more traditional approach in which the problem of a deterministic rough surface is studied first and the statistical considerations are imposed afterwards. In contrast, the scattering problem is directly considered as a stochastic boundary value problem in our approach, and all the scattered wave fields are regarded as the nonlinear functionals of the random rough surface and expanded in terms of the Wiener-Hermite functionals. As a result, we have the so-called mass operator in the denominator of the Wiener coefficients, which can be used not only to determine the effect of the rough boundary on the characteristics of the guided waves in the waveguide, but also to remove the so-called divergence difficulty in the common perturbation theory (for example, a small imaginary part of the dielectric constant has to be introduced for the numerical calculations in the perturbation theory).

The outline of the paper is as follows. In Sec. II we first investigate the structure in the absence of roughness when a plane wave is incident on it from outside. The reflection coefficient for the outgoing wave outside the waveguide and the transmission coefficient for the standing wave inside the waveguide are derived, and the dispersion properties of the guided waves supported by the structure are discussed, which will be needed and play a central role in the remainder of this paper. Then in Sec. III the stochastic representations of the scattered waves are given as expansions in terms of the complex Wiener-Hermite functionals, on the basis that the rough surface is a Gaussian random surface and has a spectral representation in terms of a Wiener integral. In Sec. IV the analytical expressions for the coefficients (the Wiener kernels) of the first three expansion terms are obtained rigorously up to second order of the surface roughness so as to satisfy the reciprocity by applying the approximate boundary conditions expanded up to third order of the random surface function. A so-called mass operator appeared in our expressions, which can be used to determine the perturbed propagation constants of the guided modes in the presence of a rough surface. The formulas for the incoherent scattering distributions are given in Sec. V. An interpretation for the scattering processes described by the Wiener kernels is also presented. The numerical results are shown and discussed in Sec. VI. Finally, the conclusions are summarized briefly in Sec. VII.

We will show that under certain conditions there are some well-pronounced peaks in the incoherent scattering distribution, in addition to the enhanced backscattering peak. These peaks mathematically come from the second-order Wiener kernel in the approximation under discussion, and such enhanced scattering can be physically interpreted as the result of an interference of the "double"-scattering processes composed of the twofold "single"-scattering processes described by the first-order Wiener kernel, which could be interpreted as a "dressed" single-scattering process.[20] The reason that the enhancement is very conspicuous in the present problem is attributable to the existence of the guided modes in the structure, since very strong interference can take place in the double-scattering processes where such guided modes appear as intermediate states. The above interpretation bears some similarity to that in Ref. 25 where the term "degenerated time-reversal symmetry" is used to interpret such enhanced scattering.

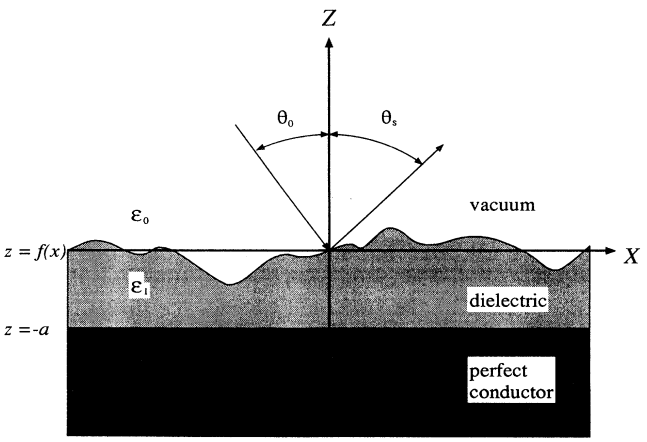

FIG. 1. The scattering structure studied in this work.

II. SOLUTIONS IN THE ABSENCE OF ROUGHNESS

Let us first study the structure in the absence of roughness. We will consider the scattering of an s-polarized electromagnetic wave, whose plane of incidence is the xz plane, which is incident from the vacuum side, as shown in Fig. 1. The electric vector of an s-polarized plane wave has only a nonzero component in the y direction, which will be denoted by ψ in what follows. The time factor $\exp(-i\omega_0 t)$ of all the fields will be suppressed for brevity.

Let ψ_i denote the incident field of a plane wave, ψ_{s0} (ψ_s) the reflected (scattered) field in the vacuum region, and ψ_{t0} (ψ_t) the transmitted (induced) field in the dielectric region, respectively. Then they have to satisfy the boundary conditions at the vacuum-dielectric interface $z=0$ $[z=f(x)]$ and the dielectric-conductor interface $z=-a$; that is, the tangential components of the electric and magnetic fields must be continuous across the interface $z=0$ $[z=f(x)]$ and the tangential component of the

electric field must vanish on the surface $z=-a$. In view of the above, these fields can be written in the form

$$\psi_i=\exp(i\lambda_0 x-i\alpha_0 z)\ , \tag{1}$$

$$\psi_{s0}=R_0\exp(i\lambda_0 x+i\alpha_0 z)\ , \tag{2}$$

$$\psi_{t0}=T_0\sin\gamma_0(z+a)\exp(i\lambda_0 x)\ , \tag{3}$$

and they have to satisfy the following conditions:

$$\psi_i+\psi_{s0}-\psi_{t0}|_{z=0}=0\ ,$$
$$\frac{\partial}{\partial z}(\psi_i+\psi_{s0}-\psi_{t0})\bigg|_{z=0}=0\ . \tag{4}$$

In Eqs. (1)–(3), $\lambda_0=k_0\sin\theta_0$ is the common propagation factor in the x direction, $\alpha_0=\sqrt{k_0^2-\lambda_0^2}=k_0\cos\theta_0$, and $\gamma_0=\sqrt{k_1^2-\lambda_0^2}$ with $k_0=\varepsilon_0^{1/2}(\omega_0/c)$ and $k_1=\varepsilon_1^{1/2}(\omega_0/c)$ being the wave numbers in the vacuum and dielectric regions, respectively, and θ_0 is the angle of incidence measuring from the z axis. The reflection and transmission coefficients R_0 and T_0 are determined by applying the boundary conditions of Eq. (4) as

$$R_0=\frac{\Delta^+(\lambda_0)}{\Delta(\lambda_0)},\quad T_0=\frac{i2\alpha_0}{\sin\gamma_0 a}\frac{1}{\Delta(\lambda_0)}\ , \tag{5}$$

$$\Delta^+(\lambda_0)=i\alpha_0+\gamma_0\cot\gamma_0 a\ , \tag{6}$$

$$\Delta(\lambda_0)=i\alpha_0-\gamma_0\cot\gamma_0 a\ . \tag{7}$$

We should point out that the common denominator $\Delta(\lambda)$ of Eq. (5) is exactly the same expression with the characteristic (dispersion) equation[25,26] obtained by solving the homogeneous wave guiding problem for the given dielectric waveguide. Indeed, the real roots of the transcendental equation $\Delta(\lambda)=0$, for a given dielectric constant $\varepsilon_r=\varepsilon_1/\varepsilon_0$ and the film thickness a, determine the surface-guided modes supported by the structure. Since the solutions of $\Delta(\lambda)=0$ have already been discussed by many authors,[25,26] we merely give a brief summary of them here. It is well known that for a guided wave propagating along the x direction, λ has to satisfy the condition $1<\lambda<\varepsilon_r$ at first. Having this in mind, a solvability examination of $\Delta(\lambda)=0$ shows that the structure can support no guided mode for

$$0<U<\frac{\pi}{2}\ , \tag{8a}$$

one guided mode for

$$\frac{\pi}{2}<U<\frac{3\pi}{2}\ , \tag{8b}$$

two guided modes for

$$\frac{3\pi}{2}<U<\frac{5\pi}{2}\ , \tag{8c}$$

and, in general, n guided modes for

$$\frac{(2n-1)\pi}{2}<U<\frac{(2n+1)\pi}{2}\ , \tag{8d}$$

where $U=\sqrt{\varepsilon_r-1}k_0 a$ is the normalized waveguide parameter. It should be noted that in the case of the absence of roughness, no guided mode can be excited by an incident wave from the vacuum side since $\lambda_0<1$. However, in the case of the existence of a rough surface, the guided waves could be excited if the structure can support them. The guided modes will play an important role in the scattering as we see in the following sections.

III. STOCHASTIC REPRESENTATION FOR SCATTERED WAVES

We now consider the structure with a one-dimensional, randomly rough surface expressed by $z=f(x;\omega)$, where $f(x;\omega)$ is a random function with the mean $\langle f(x;\omega)\rangle=0$. In this notation, ω denotes a sample point in the sample space Ω, which is the ensemble of the realizations of f, and the angle brackets $\langle\ \rangle$ indicate the probabilistic average over Ω. If $f(x;\omega)$ is a homogeneous Gaussian random function on the planar surface, then as shown in previous papers[10–15] we have the spectral representation of $f(x;\omega)$ in terms of a Wiener integral:

$$f(x;\omega)=\int_{-\infty}^{+\infty}e^{i\lambda x}F(\lambda)dB(\lambda)\ , \tag{9}$$

where we have put $dB(\lambda)\equiv dB(\lambda;\omega)$, and will delete ω for brevity in what follows. Here $dB(\lambda)$ denotes the complex Gaussian random measure with the properties

$$\langle dB(\lambda)\rangle=0,\quad dB^*(\lambda)=dB(-\lambda)\ ,$$
$$\langle dB(\lambda)dB^*(\lambda')\rangle=\delta(\lambda-\lambda')d\lambda d\lambda'\ , \tag{10}$$

where the $*$ indicates the complex conjugate. From Eq. (9) and by making use of Eq. (10), we have the following expressions for the correlation function:

$$R(x)=\langle f(x+x';\omega)f(x';\omega)\rangle$$
$$=\int_{-\infty}^{+\infty}e^{i\lambda x}|F(\lambda)|^2 d\lambda \tag{11}$$

and the variance of the roughness that describes the random surface

$$\sigma^2=R(0)=\int_{-\infty}^{+\infty}|F(\lambda)|^2 d\lambda\ , \tag{12}$$

where we have used the relation $F(\lambda)=F^*(-\lambda)$. $|F(\lambda)|^2$ is called the power spectrum of the random planar surface. $|F(\lambda)|^2=0$ and then $\sigma^2=0$ correspond to an ideal smooth (flat) surface.

It is obvious that the wave fields will be perturbed and become random as the top boundary is statistically a rough surface, and there are also waves scattered into various directions (incoherent scattering) in the vacuum region, in addition to the "specular" direction (coherent scattering), as well as the induced standing waves with various wave numbers and the surface-guided waves in the dielectric region. Regarding the problem as a random boundary value problem, we can express the scattered and induced wave fields as stochastic functionals of the random surface function $f(x;\omega)$. And if we suppose that $f(x;\omega)$ is a homogeneous Gaussian random function, then just as what has been shown in previous papers,[10–15,20] the random wave fields are the eigenfunctions of a shift operator D^x with the eigenvalue $e^{i\lambda x}$ (here

D^x is defined by a translation in the x direction and denotes the measure-preserving transformation in the sample space Ω; see Refs. 14 and 20 for details). Thus, in view of the form of Eqs. (2) and (3), we can expand the scattered field $\psi_s(x,z;\omega)$ in the vacuum region and the induced field $\psi_t(x,z;\omega)$ in the dielectric region (here ω denotes that they are random fields) in terms of the Wiener-Hermite functionals in the following manner:

$$\psi_s(x,z;\omega)=A_0(\lambda_0)e^{i\lambda_0 x+i\alpha_0 z}+\sum_{n=1}^{\infty}\int_{-\infty}^{+\infty}\int_{-\infty}^{+\infty}\cdots\int_{-\infty}^{+\infty}A_n(\lambda_1,\lambda_2,\ldots,\lambda_n|\lambda_0)\times e^{i\eta_n x+i\alpha_n z}\hat{h}_n[dB(\lambda_1),dB(\lambda_2),\ldots,dB(\lambda_n)]\,, \tag{13}$$

$$\psi_t(x,z;\omega)=C_0(\lambda_0)\sin\gamma_0(z+a)e^{i\lambda_0 x}+\sum_{n=1}^{\infty}\int_{-\infty}^{+\infty}\int_{-\infty}^{+\infty}\cdots\int_{-\infty}^{+\infty}C_n(\lambda_1,\lambda_2,\ldots,\lambda_n|\lambda_0)\times\sin\gamma_n(z+a)e^{i\eta_n x}\hat{h}_n[dB(\lambda_1),dB(\lambda_2),\ldots,dB(\lambda_n)]\,, \tag{14}$$

with

$$\eta_n=\lambda_0+\lambda_1+\cdots+\lambda_n\,, \tag{15}$$

which can be interpreted as a composed wave number originated from the scattering process of the rough boundary. α_n and γ_n are defined as $\alpha_n=\sqrt{k_0^2-\eta_n^2}$ and $\gamma_n=\sqrt{k_1^2-\eta_n^2}$. $\hat{h}_n[\cdots]$ denotes the nth degree complex Wiener-Hermite differential, which is to be understood as a generalization of Hermite polynomial (notice $\hat{h}_0=1$). The Wiener-Hermite differentials satisfy the following recurrence and orthogonality relations:[5,10–20,27]

$$dB(\lambda)\cdot\hat{h}_n[dB(\lambda_1),dB(\lambda_2),\ldots,dB(\lambda_n)]=\hat{h}_{n+1}[dB(\lambda),dB(\lambda_1),dB(\lambda_2),\ldots,dB(\lambda_n)]+\sum_{i=1}^{n}\hat{h}_{n-1}[dB(\lambda_1),\ldots,dB(\lambda_{i-1}),dB(\lambda_{i+1}),\ldots,dB(\lambda_n)]\times\delta(\lambda+\lambda_i)d\lambda d\lambda_i\,, \tag{16}$$

$$\langle\hat{h}_n[dB(\lambda_{i_1}),\ldots,dB(\lambda_{i_n})]\cdot\hat{h}_m[dB(\lambda_{j_1}),\ldots,dB(\lambda_{j_m})]\rangle=\delta_{nm}\delta_{ij}^{n}d\lambda_{i_1}\cdots d\lambda_{i_n}d\lambda_{j_1}\cdots d\lambda_{j_m}\,, \tag{17}$$

where δ_{nm} is Kronecker's delta and δ_{ij}^{n} denotes the sum of all distinct products of n delta functions of the form $\delta(\lambda_{i_\nu}+\lambda_{i_\mu})$, $i=(i_1,i_2,\ldots,i_n)$, $j=(j_1,j_2,\ldots,j_m)$, all i_ν and j_μ appearing just once in each product.

The integrals of Eqs. (13) and (14) represent the n-tuple complex Wiener integrals, and can be regarded as the stochastic representations for the scattered and induced fields. The Wiener coefficients A_n's and C_n's are the unknown integral kernels to be determined by applying the boundary condition on the rough boundary. Once the kernels are obtained, we can even draw a spatial realization of the stochastic wave fields corresponding to a given realization of the random surface. On the other hand, we can easily calculate various statistical quantities of the random wave fields by means of an averaging procedure. We only show here the coherent and incoherent part of the fields. By taking the average of Eq. (13) and Eq. (14), the coherent or average fields are given by

$$\psi_{sc}=\langle\psi_s\rangle=A_0(\lambda_0)e^{i\lambda_0 x+i\alpha_0 z}\,, \tag{18}$$

$$\psi_{tc}=\langle\psi_t\rangle=C_0(\lambda_0)\sin\gamma_0(z+a)e^{i\lambda_0 x}\,, \tag{19}$$

where the constant $A_0(\lambda_0)$ is the 0th Wiener kernel. It is obvious that the coherent scattering takes place in the direction of specular reflection, so $A_0(\lambda_0)$ represents also the reflection coefficient of the random surface.

The incoherent fields are then obtained by subtracting the coherent parts from the total fields. Let $P(\theta_s|\theta_0)$ denote the angular distribution of the incoherent scattering, that is, the average power flow scattered incoherently from unit surface area into unit solid angle of the direction θ_s when the angle of incidence is θ_0, we have[20]

$$P(\theta_s|\theta_0)=\sum_{n=1}^{\infty}P_n(\theta_s|\theta_0)=k_0\cos^2\theta_s\left[|A_1(\lambda_s-\lambda_0|\lambda_0)|^2+2!\int_{-\infty}^{+\infty}|A_2(\lambda_s-\lambda_0-\lambda_2,\lambda_2|\lambda_0)|^2d\lambda_2+\cdots\right]\,, \tag{20}$$

where $P_n(\theta_s|\theta_0)$ represents the contribution from A_n, $\lambda_s=k_0\sin\theta_s$. As we have shown in Ref. 20, from the reciprocal

relations held by the Wiener kernels, the incoherent distribution $P(\theta_s|\theta_0)$ has also the reciprocity

$$P(\theta_s|\theta_0)=P(\theta_0|\theta_s)\ . \tag{21}$$

IV. APPROXIMATION SOLUTION FOR THE WIENER COEFFICIENTS

To investigate the coherent and incoherent scattering in detail, we have to determine the Wiener expansion coefficients A_n's and C_n's by applying the boundary condition at the random boundary $z=f(x;\omega)$; that is, the tangential components of the electric and magnetic fields must be continuous across the interface $z=f(x;\omega)$. For simplicity and only to demonstrate the usefulness of the stochastic functional approach, we here confine ourselves to the case that the random boundary is slightly rough, that is $\sigma^2\ll 1$. In this case, the boundary conditions can be approximated by expanding them as the Taylor series in terms of f and $\nabla f=(df/dx)\hat{x}$. To obtain only the first three kernels $A_0(C_0)$, $A_1(C_1)$, and $A_2(C_2)$, and also to satisfy the reciprocity, it is sufficient to expand the boundary conditions up to third order of the surface functions (f or df/dx or their multiplication). Therefore, we have the approximate boundary conditions as follows:

$$\left.\psi+f\frac{\partial\psi}{\partial z}+\frac{f^2}{2}\frac{\partial^2\psi}{\partial z^2}+\frac{f^3}{6}\frac{\partial^3\psi}{\partial z^3}\right|_{z=0}=0\ , \tag{22}$$

$$\left.\frac{\partial\psi}{\partial z}-\frac{df}{dx}\frac{\partial\psi}{\partial x}+f\frac{\partial^2\psi}{\partial z^2}-f\frac{df}{dx}\frac{\partial^2\psi}{\partial x\partial z}+\frac{f^2}{2}\frac{\partial^3\psi}{\partial z^3}+\frac{f^3}{6}\frac{\partial^4\psi}{\partial z^4}-\frac{f^2}{2}\frac{df}{dx}\frac{\partial^3\psi}{\partial x\partial z^2}\right|_{z=0}=0\ , \tag{23}$$

where $\psi=\psi_i+\psi_s-\psi_t$. Substituting the fields into Eqs. (22) and (23), and making use of the recurrence formula and the orthogonality relation for $\hat{h}_n$,[10,11,27] we consequently obtain a set of hierarchical equations for the Wiener coefficients as follows. For $n=0$:

$$\left[1-\frac{\alpha_0^2\sigma^2}{2}\right](A_0+1)-\left[1-\frac{\gamma_0^2\sigma^2}{2}\right]\sin\gamma_0 aC_0+\int_{-\infty}^{+\infty}[i\alpha_1A_1-\gamma_1\cos\gamma_1 aC_1]F^*(\lambda_1)d\lambda_1=0\ , \tag{24}$$

$$\left[1-\frac{\alpha_0^2\sigma^2}{2}\right]i\alpha_0(A_0-1)-\left[1-\frac{\gamma_0^2\sigma^2}{2}\right]\gamma_0\cos\gamma_0 aC_0 - \int_{-\infty}^{+\infty}[(\alpha_1^2+\eta_1\lambda_1)A_1-(\gamma_1^2+\eta_1\lambda_1)\sin\gamma_1 aC_1]F^*(\lambda_1)d\lambda_1=0\ . \tag{25}$$

For $n=1$:

$$\left[1-\frac{\alpha_1^2\sigma^2}{2}\right]A_1-\left[1-\frac{\gamma_1^2\sigma^2}{2}\right]\sin\gamma_1 aC_1-F(\lambda_1)\int_{-\infty}^{+\infty}[\alpha_1^2(\lambda_2)A_1(\lambda_2)-\gamma_1^2(\lambda_2)\sin\gamma_1(\lambda_2)aC_1(\lambda_2)]F^*(\lambda_2)d\lambda_2$$
$$+F(\lambda_1)\left[\left[1-\frac{\alpha_0^2\sigma^2}{2}\right]i\alpha_0(A_0-1)-\left[1-\frac{\gamma_0^2\sigma^2}{2}\right]\gamma_0\cos\gamma_0 aC_0\right]+2\int_{-\infty}^{+\infty}[i\alpha_2A_2-\gamma_2\cos\gamma_2 aC_2]F^*(\lambda_2)d\lambda_2=0\ , \tag{26}$$

$$\left[1-\frac{\alpha_1^2\sigma^2}{2}\right]i\alpha_1A_1-\left[1-\frac{\gamma_1^2\sigma^2}{2}\right]\gamma_1\cos\gamma_1 aC_1$$
$$-F(\lambda_1)\int_{-\infty}^{+\infty}\{[\alpha_1^2(\lambda_2)+\eta_1(\lambda_2)\lambda_2-\lambda_0\lambda_1]i\alpha_1(\lambda_2)A_1(\lambda_2)$$
$$-[\gamma_1^2(\lambda_2)+\eta_1(\lambda_2)\lambda_2-\lambda_0\lambda_1]\gamma_1(\lambda_2)\cos\gamma_1(\lambda_2)aC_1(\lambda_2)\}F^*(\lambda_2)d\lambda_2$$
$$-F(\lambda_1)\left[\left[1-\frac{\alpha_0^2\sigma^2}{2}\right](\alpha_0^2-\lambda_0\lambda_1)(A_0+1)-\left[1-\frac{\gamma_0^2\sigma^2}{2}\right](\gamma_0^2-\lambda_0\lambda_1)\sin\gamma_0 aC_0\right]$$
$$-2\int_{-\infty}^{+\infty}[(\alpha_2^2+\eta_2\lambda_2)A_2-(\gamma_2^2+\eta_2\lambda_2)\sin\gamma_2 aC_2]F^*(\lambda_2)d\lambda_2=0\ . \tag{27}$$

For $n=2$:

$$\left[1-\frac{\alpha_2^2\sigma^2}{2}\right]A_2-\left[1-\frac{\gamma_2^2\sigma^2}{2}\right]\sin\gamma_2 aC_2-[\alpha_0^2(A_0+1)-\gamma_0^2\sin\gamma_0 aC_0]F(\lambda_1)F(\lambda_2)/2$$

$$+[i\alpha_1(\lambda_1)A_1(\lambda_1)-\gamma_1(\lambda_1)\cos\gamma_1(\lambda_1)aC_1(\lambda_1)]F(\lambda_2)/2$$

$$+[i\alpha_1(\lambda_2)A_1(\lambda_2)-\gamma_1(\lambda_2)\cos\gamma_1(\lambda_2)aC_1(\lambda_2)]F(\lambda_1)/2$$

$$+3\int_{-\infty}^{+\infty}[i\alpha_3 A_3-\gamma_3\cos\gamma_3 aC_3]F^*(\lambda_3)d\lambda_3=0\ , \tag{28}$$

$$\left[1-\frac{\alpha_2^2\sigma^2}{2}\right]i\alpha_2 A_2-\left[1-\frac{\gamma_2^2\sigma^2}{2}\right]\gamma_2\cos\gamma_2 aC_2$$

$$-\{[\alpha_0^2-\lambda_0(\lambda_1+\lambda_2)]i\alpha_0(A_0-1)-[\gamma_0^2-\lambda_0(\lambda_1+\lambda_2)]\gamma_0\cos\gamma_0 aC_0\}F(\lambda_1)F(\lambda_2)/2$$

$$-\{[\alpha_1^2(\lambda_1)-\eta_1(\lambda_1)\lambda_2]A_1(\lambda_1)-[\gamma_1^2(\lambda_1)-\eta_1(\lambda_1)\lambda_2]\sin\gamma_1(\lambda_1)aC_1(\lambda_1)\}F(\lambda_2)/2$$

$$-\{[\alpha_1^2(\lambda_2)-\eta_1(\lambda_2)\lambda_1]A_1(\lambda_2)-[\gamma_1^2(\lambda_2)-\eta_1(\lambda_2)\lambda_1]\sin\gamma_1(\lambda_2)aC_1(\lambda_2)\}F(\lambda_1)/2$$

$$-3\int_{-\infty}^{+\infty}[(\alpha_3^2+\eta_3\lambda_3)A_3-(\gamma_3^2+\eta_3\lambda_3)\sin\gamma_3 aC_3]F^*(\lambda_3)d\lambda_3=0\ . \tag{29}$$

For $n=3$:

$$\left[1-\frac{\alpha_3^2\sigma^2}{2}\right]A_3-\left[1-\frac{\gamma_3^2\sigma^2}{2}\right]\sin\gamma_3 aC_3-[i\alpha_0^3(A_0-1)-\gamma_0^3\cos\gamma_0 aC_0]F(\lambda_1)F(\lambda_2)F(\lambda_3)/6$$

$$-[\alpha_1^2(\lambda_1)A_1(\lambda_1)-\gamma_1^2(\lambda_1)\sin\gamma_1(\lambda_1)aC_1(\lambda_1)]F(\lambda_2)F(\lambda_3)/6$$

$$-[\alpha_1^2(\lambda_2)A_1(\lambda_2)-\gamma_1^2(\lambda_2)\sin\gamma_1(\lambda_2)aC_1(\lambda_2)]F(\lambda_1)F(\lambda_3)/6$$

$$-[\alpha_1^2(\lambda_3)A_1(\lambda_3)-\gamma_1^2(\lambda_3)\sin\gamma_1(\lambda_3)aC_1(\lambda_3)]F(\lambda_1)F(\lambda_2)/6$$

$$+[i\alpha_2(\lambda_1,\lambda_2)A_2(\lambda_1,\lambda_2)-\gamma_2(\lambda_1,\lambda_2)\cos\gamma_2(\lambda_1,\lambda_2)aC_2(\lambda_1,\lambda_2)]F(\lambda_3)/3$$

$$+[i\alpha_2(\lambda_1,\lambda_3)A_2(\lambda_1,\lambda_3)-\gamma_2(\lambda_1,\lambda_3)\cos\gamma_2(\lambda_1,\lambda_3)aC_2(\lambda_1,\lambda_3)]F(\lambda_2)/3$$

$$+[i\alpha_2(\lambda_2,\lambda_3)A_2(\lambda_2,\lambda_3)-\gamma_2(\lambda_2,\lambda_3)\cos\gamma_2(\lambda_2,\lambda_3)aC_2(\lambda_2,\lambda_3)]F(\lambda_1)/3$$

$$+4\int_{-\infty}^{+\infty}[i\alpha_4 A_4-\gamma_4\cos\gamma_4 aC_4]F^*(\lambda_4)d\lambda_4=0\ , \tag{30}$$

$$\left[1-\frac{\alpha_3^2\sigma^2}{2}\right]i\alpha_3 A_3-\left[1-\frac{\gamma_3^2\sigma^2}{2}\right]\gamma_3\cos\gamma_3 aC_3$$

$$+\{\alpha_0^2[\alpha_0^2-\lambda_0(\lambda_1+\lambda_2+\lambda_3)](A_0+1)-\gamma_0^2[\gamma_0^2-\lambda_0(\lambda_1+\lambda_2+\lambda_3)]\sin\gamma_0 aC_0\}\frac{F(\lambda_1)F(\lambda_2)F(\lambda_3)}{6}$$

$$-\{[\alpha_1^2(\lambda_1)-\eta_1(\lambda_1)(\lambda_2+\lambda_3)]i\alpha_1(\lambda_1)A_1(\lambda_1)$$

$$-[\gamma_1^2(\lambda_1)-\eta_1(\lambda_1)(\lambda_2+\lambda_3)]\gamma_1(\lambda_1)\cos\gamma_1(\lambda_1)aC_1(\lambda_1)\}F(\lambda_2)F(\lambda_3)/6$$

$$-\{[\alpha_1^2(\lambda_2)-\eta_1(\lambda_2)(\lambda_1+\lambda_3)]i\alpha_1(\lambda_2)A_1(\lambda_2)-[\gamma_1^2(\lambda_2)-\eta_1(\lambda_2)(\lambda_1+\lambda_3)]\gamma_1(\lambda_2)\cos\gamma_1(\lambda_2)aC_1(\lambda_2)\}F(\lambda_1)F(\lambda_3)/6$$

$$-\{[\alpha_1^2(\lambda_3)-\eta_1(\lambda_3)(\lambda_1+\lambda_2)]i\alpha_1(\lambda_3)A_1(\lambda_3)-[\gamma_1^2(\lambda_3)-\eta_1(\lambda_3)(\lambda_1+\lambda_2)]\gamma_1(\lambda_3)\cos\gamma_1(\lambda_3)aC_1(\lambda_3)\}F(\lambda_1)F(\lambda_2)/6$$

$$-\{[\alpha_2^2(\lambda_1,\lambda_2)-(\lambda_0+\lambda_1+\lambda_2)\lambda_3]A_2(\lambda_1,\lambda_2)-[\gamma_2^2(\lambda_1,\lambda_2)-(\lambda_0+\lambda_1+\lambda_2)\lambda_3]\sin\gamma_2(\lambda_1,\lambda_2)aC_2(\lambda_1,\lambda_2)\}F(\lambda_3)/3$$

$$-\{[\alpha_2^2(\lambda_1,\lambda_3)-(\lambda_0+\lambda_1+\lambda_3)\lambda_2]A_2(\lambda_1,\lambda_3)-[\gamma_2^2(\lambda_1,\lambda_3)-(\lambda_0+\lambda_1+\lambda_3)\lambda_2]\sin\gamma_2(\lambda_1,\lambda_3)aC_2(\lambda_1,\lambda_3)\}F(\lambda_2)/3$$

$$-\{[\alpha_2^2(\lambda_2,\lambda_3)-(\lambda_0+\lambda_2+\lambda_3)\lambda_1]A_2(\lambda_2,\lambda_3)-[\gamma_2^2(\lambda_2,\lambda_3)-(\lambda_0+\lambda_2+\lambda_3)\lambda_1]\sin\gamma_2(\lambda_2,\lambda_3)aC_2(\lambda_2,\lambda_3)\}F(\lambda_1)/3$$

$$-4\int_{-\infty}^{+\infty}[(\alpha_4^2+\eta_4\lambda_4)A_4-(\gamma_4^2+\eta_4\lambda_4)\sin\gamma_4 aC_4]F^*(\lambda_4)d\lambda_4=0\ , \tag{31}$$

where we have abbreviated $A_n(\cdots)$ and $C_n(\cdots)$ by A_n and C_n, and omitted the equations for $n\geq 4$ for brevity. The notations $\eta_1(\lambda_2)$, $\alpha_1(\lambda_2)$, $\gamma_1(\lambda_2)$, $A_1(\lambda_2)$, and $C_2(\lambda_2)$ mean to replace λ_1 by λ_2 in their expressions. Solving the above equations by an approximate procedure similar to that used in our previous works,[5,6] we finally lead to the following approximate solutions for the coefficients of the first three terms A_0, A_1, and A_2 as

$$A_0(\lambda_0)=[\Delta^+(\eta_0)+MA_0(\eta_0)]/Q(\eta_0)\ , \tag{32}$$

$$A_1(\lambda_1|\lambda_0)=\frac{i2\alpha_0 VF(\lambda_1)}{Q(\eta_0)Q(\eta_1)}[1+MA_1(\eta_1,\eta_0)]$$

$$=A_1^{(0)}(\lambda_1|\lambda_0)[1+MA_1(\eta_1,\eta_0)]\ , \tag{33}$$

$$A_2(\lambda_1,\lambda_2|\lambda_0)=\frac{i\alpha_0 VF(\lambda_1)F(\lambda_2)}{Q(\eta_0)Q(\eta_2)}\left[\frac{V}{Q(\lambda_0+\lambda_1)}+\frac{V}{Q(\lambda_0+\lambda_2)}-(\gamma_0\cot\gamma_0 a+\gamma_2\cot\gamma_2 a)\right] \tag{34}$$

$$=-\frac{V}{2Q(\eta_2)}[A_1^{(0)}(\lambda_1|\lambda_0)F(\lambda_2)+A_1^{(0)}(\lambda_2|\lambda_0)F(\lambda_1)]-\frac{i\alpha_0 VF(\lambda_1)F(\lambda_2)}{Q(\eta_0)Q(\eta_2)}[\gamma_0\cot\gamma_0 a+\gamma_2\cot\gamma_2 a]\ , \tag{35}$$

with

$$Q(\eta)=\Delta(\eta)+M(\eta)\ , \tag{36}$$

$$M(\eta)=\left[\frac{V\sigma^2}{2}+\gamma^2(\eta)\sigma^2+G_2(\eta)\right]\Delta(\eta)$$

$$+V\sigma^2\gamma(\eta)\cot\gamma(\eta)a-VG_1(\eta)\ , \tag{37}$$

$$MA_0(\eta_0)=\frac{V\sigma^2}{2}\Delta(\eta_0)+[\gamma_0^2\sigma^2+G_2(\eta_0)]\Delta^+(\eta_0)$$

$$+VG_1(\eta_0)\ , \tag{38}$$

$$MA_1(\eta_0,\eta_1)=\frac{(\gamma_0^2+\gamma_1^2)\sigma^2}{2}+\gamma_0\gamma_1\sigma^2\cot\gamma_0 a\cot\gamma_1 a$$

$$-[\gamma_0\cot\gamma_0 aG_1(\eta_1)+\gamma_1\cot\gamma_1 aG_1(\eta_0)]$$

$$+G_3(\eta_0,\eta_1)\ , \tag{39}$$

and

$$G_1(\eta)=\int_{-\infty}^{+\infty}\frac{V}{Q(\lambda)}|F(\lambda-\eta)|^2 d\lambda\ , \tag{40}$$

$$G_2(\eta)=\int_{-\infty}^{+\infty}\frac{V\gamma(\lambda)\cot\gamma(\lambda)a}{Q(\lambda)}|F(\lambda-\eta)|^2 d\lambda\ , \tag{41}$$

$$G_3(\eta_0,\eta_1)=\int_{-\infty}^{+\infty}\frac{V}{Q(\eta_0+\lambda)}\frac{V}{Q(\eta_1+\lambda)}|F(\lambda)|^2d\lambda\ , \quad (42)$$

where $\gamma(\lambda)=\sqrt{k_1^2-\lambda^2}$, $V=k_0^2(\varepsilon_r-1)$, and the definitions of the other notations or parameters have been given in the previous sections. We are not concerned with the coefficients C_n's in the present paper, so we do not give their expressions here for brevity.

It can be seen that a factor $M(\eta)$ has been involved in the denominators of our expressions for the Wiener kernels, which satisfies the iterative integral equation given by Eq. (37) and is of the order of σ^2. Since $M(\eta)$ plays a similar role as a mass operator in the graphical or Feynman diagrammatic method[2] for the scattering problems in random media or from rough surfaces, we will also call it the mass operator. To get the exact values of the mass operator, we have to solve an integral equation. However, we can approximately evaluate the mass operator by neglecting it in the denominator of its integrand as done in what follows, although we can obtain better values in an iterative way if it is necessary. As we have shown in previous works,[5,6] the mass operator $M(\eta)$ can be used to determine the perturbed propagation constants of the guided modes that are modified due to the rough surface. If the roughness is small enough, the perturbed propagation constants can be regarded as small corrections to the unperturbed ones, we then have the following expression:

$$\delta\beta_n=\tilde{\beta}_n-\beta_n=-\left.\frac{M(\eta)}{d\Delta(\eta)/d\eta}\right|_{\eta=\beta_n}\ , \quad (43)$$

where $\tilde{\beta}_n$, the roots of $Q(\eta)=\Delta(\eta)+M(\eta)=0$, stands for the perturbed propagation constants; and β_n, the roots of $\Delta(\eta)=0$, stands for the unperturbed propagation constants of the guided modes. Furthermore, because $\tilde{\beta}_n$ is always complex even for a real dielectric constant ε_r, unlike that in the common perturbation theory,[25] in our theory it is not necessary to introduce a small imaginary part in the dielectric constant in order to remove the so-called divergence difficulty for the numerical calculations.

V. INCOHERENT SCATTERING DISTRIBUTION

By substituting A_1 and A_2 given by Eqs. (33) and (34) into Eq. (20), we obtain the incoherent scattering distribution as

$$P(\theta_s|\theta_0)=P_1(\theta_s|\theta_0)+P_2(\theta_2|\theta_0)\ , \quad (44)$$

where P_1, the contribution from A_1, is given by

$$P_1(\theta_s|\theta_0)=\frac{4k_0^3|V|^2\cos^2\theta_0\cos^2\theta_s}{|Q(\lambda_0)Q(\lambda_s)|^2}\times|1+MA_1(\lambda_0,\lambda_2)|^2|F(\lambda_s-\lambda_0)|^2 \quad (45)$$

and P_2, the contribution from A_2, is given by

$$P_2(\theta_s|\theta_0)=\frac{2k_0^3|V|^2\cos^2\theta_0\cos^2\theta_s}{|Q(\lambda_0)Q(\lambda_s)|^2}\int_{-\infty}^{+\infty}\left|\frac{V}{Q(\lambda)}+\frac{V}{Q(\lambda_0+\lambda_s-\lambda)}-(\gamma_0\cot\gamma_0 a+\gamma_s\cot\gamma_s a)\right|^2\times|F(\lambda-\lambda_0)F(\lambda_s-\lambda)|^2d\lambda\ , \quad (46)$$

where $\lambda_0=k_0\sin\theta_0$, $\lambda_s=k_0\sin\theta_s$, $\gamma_0=k_0\sqrt{\varepsilon_r-\sin^2\theta_0}$, and $\gamma_s=k_0\sqrt{\varepsilon_r-\sin^2\theta_s}$. It should be noted that although we have just considered the contributions from the Wiener kernels only up to second order, a part of the contributions from higher orders has been involved due to the mass operator. In addition, we hope to point out that our results really are the same as those obtained by the perturbation theory[25] if we expand them in terms of the powers of the surface roughness σ^2 and merely retain the terms up to second order σ^4 [notice that $M(\lambda)$ and $|F(\lambda)|^2$ are of the order of σ^2]. In fact, after doing so, we can easily find that our $P_1(\theta_s|\theta_0)$ corresponds to the sum of $I_2(p|k)$ and $I_4^{(1-3)}(p|k)$ in Ref. 25, and $P_2(\theta_s|\theta_0)$ corresponds to the sum of $I_4^{(2-2)L}(p|k)$ and $I_4^{(2-2)C}(p|k)$. It is then clear that even $P_1(\theta_s|\theta_0)$ already involves higher-order terms than σ^2, which are usually interpreted as the result of the multiple-scattering processes. Therefore, we may interpret the first Wiener kernel $A_1(\lambda_s-\lambda_0|\lambda_0)$ as describing a "renormalized" or "dressed" single-scattering process, which we express symbolically as $\{\lambda_0\rightarrow\lambda_s\}$ [see Fig. 2(a)].

As shown in the numerical calculations discussed in the next section, there are enhanced peaks on the incoherent scattering distribution in the backward scattering direction, and in some additional directions when the structure can support more than two guided modes. The calculations also show that these peaks come from P_2 given by the integral of the second-order kernel A_2, which involves two terms related to A_1 as in Eq. (35). By rewriting Eq. (35) in the following way:

$$A_2(\lambda_s-\lambda,\lambda-\lambda_0|\lambda_0)=-V/2\dot{Q}(\lambda_s)(\{A_1^{(0)}(\lambda_s-\lambda|\lambda_0)F(\lambda-\lambda_0)+A_1^{(0)}[\lambda_s-(\lambda_0+\lambda_s-\lambda)|\lambda_0]F[(\lambda_0+\lambda_s-\lambda)-\lambda_0]\}+[i2\alpha_0F(\lambda_s-\lambda)F(\lambda-\lambda_0)/Q(\lambda_0)][\gamma_0\cot\gamma_0 a+\gamma_s\cot\gamma_s a])\ , \quad (47)$$

and with the interpretation for the first-order kernel A_1 in mind, we may interpret that the process described by A_2 involves two double-scattering processes: the first one gives the double-scattering process $\{\lambda_0\rightarrow\lambda\rightarrow\lambda_s\}$, and the second is $\{\lambda_0\rightarrow(\lambda_s+\lambda_0-\lambda)\rightarrow\lambda_s\}$ [see Fig. 2(b)]. Thus, P_2 of Eq. (44) consists of the integration over intermediate states.

If there are some steady propagating states existing in

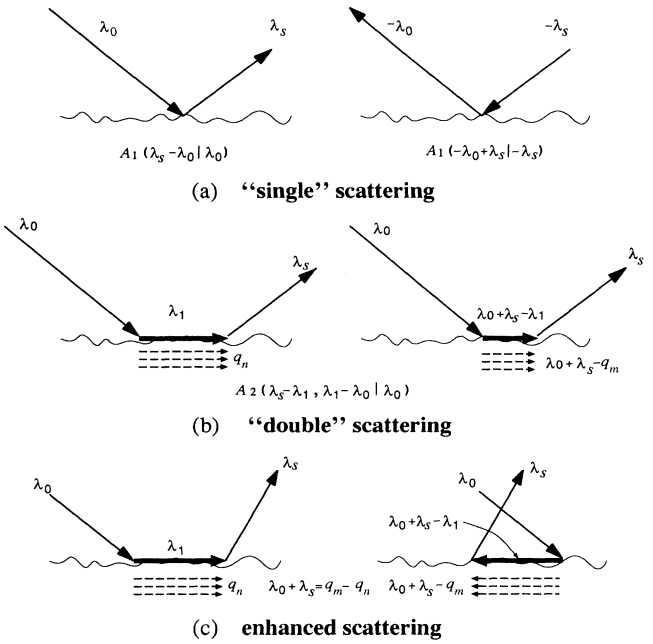

FIG. 2. Scattering diagrams for "single"- and "double"-scattering processes. (a) Single-scattering processes $\{\lambda_0 \rightarrow \lambda_s\}$ described by A_1 and its reciprocal process $\{-\lambda_0 \rightarrow -\lambda_s\}$. (b) Two double-scattering processes described by A_2. A thick arrow shows an intermediate state. (c) Enhanced double-scattering processes for the certain direction with $\lambda_0+\lambda_s=q_m-q_n$.

the structure as intermediate states, then the two double-scattering processes can interfere with each other to produce the so-called enhanced scattering under certain conditions. Such steady states are mathematically given by the poles in A_2, and they physically correspond to the guided modes supported by the structure in our problem under discussion. As shown in Fig. 2(c), denoting by q_n ($n=1,2,\ldots$) the propagation constants (real part) of the guided modes, the enhanced scattering will take place at

$$\lambda_s = -\lambda_0 + q_m - q_n \tag{48}$$

and in the language of the angle, Eq. (46) is in the form

$$\sin\theta_s = -\sin\theta_0 + (q_m - q_n)/k_0 , \tag{49}$$

which means the backward direction when $q_m = q_n$, and the additional directions when $q_m \neq q_n$. Of course, $|(q_m - q_n)/k_0|$ should not be too large (at least <2) since the scattering angle θ_s has to satisfy the condition $-90° < \theta_s < +90°$.

On the other hand, since the enhanced peaks in the incoherent distribution arise from the interference between the peaks at the surface wave poles in two groups in which the positions of the poles of one group are connected with λ_s (in other words, the scattering angle), so the widths of the enhanced peaks are related to the widths of the peaks at the poles, that means we can roughly estimate the widths of the enhanced peaks from the widths of the peaks at the poles. It is well known that the widths of the peaks at the poles are dependent on the attenuation constants (the imaginary part of the propagation constant, denoted by p_n in what follows) of the guided modes. We show in Fig. 3 the integrand of P_2 as a function of its integral variable λ/k_0 with λ_s/k_0 a parameter for the case where the structure can support two guided modes (the form of the power spectrum of the rough surface used in the calculation is given in Sec. VI). It is clear that the enhanced backscattering peak is due to the interference between the modes in the same orders and the enhanced satellite peaks are due to that between the modes in the different orders. The interference is mainly controlled by the peak with the larger amplitude, for example, the peak of the second-order mode in the case of Fig. 3, and hence the widths of the enhanced peaks are

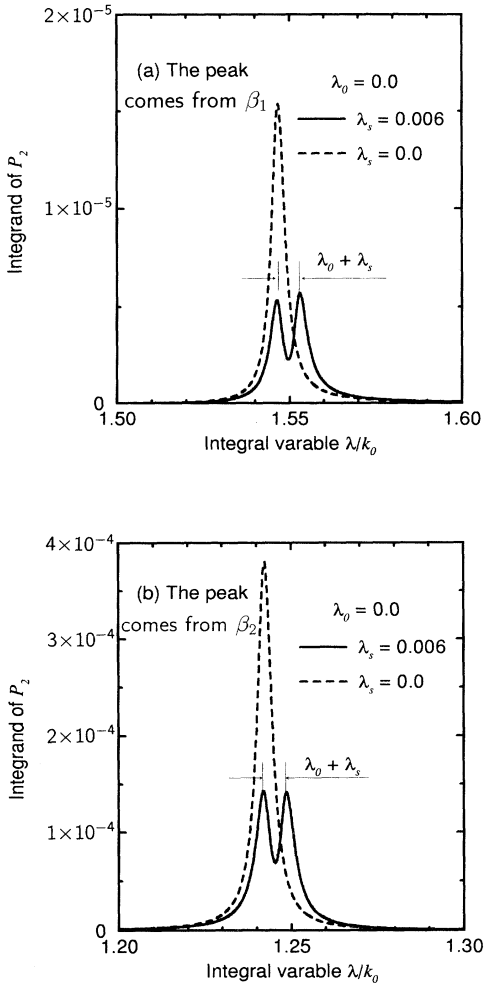

FIG. 3. The peaks in the integrand of P_2 as a function of λ with different values of λ_s (neglecting the mass operator). The parameters used in calculation are $a=500$ (the wavelength 632.8), $\varepsilon_r = 2.6896 + i0.0075$, $\sigma/a = 0.03$, and $l/a = 0.1$. The structure can support two guided modes. (a) The peaks come from the first-order mode, and (b) the peaks come from the second-order mode.

mainly determined by the width of this larger peak. Assuming that two peaks do not interfere with each other after the difference of their positions is twice the width of the larger peak, then the width of the enhanced peak due to the interference of those two peaks is about four times the width of the larger peak. (Exactly, the enhanced peaks are related to the interference of the peaks at the poles by an integration, so it is not easy to give an explicit relationship between their widths. The above arguments are merely intuitive and rough.) Denoting by θ_w the width of the enhanced peaks and by p_w the attenuation constant of the mode that gives rise to the largest peaks in the integrand of P_2, we then have the following expression for roughly estimating the width of the enhanced peaks:

$$\theta_w = \arcsin(4p_w/k_0) \ . \tag{50}$$

If $p_w = 0$, that is, no attenuation for the guided modes, then the width of the enhanced peaks will be zero. As stated in Ref. 25, to calculate the incoherent scattering distribution, especially the contribution from A_2, a small imaginary part of the dielectric constant has to be introduced to yield a finite width to each of the enhanced peaks in the perturbation theory. Otherwise, the perturbation theory will give out the peaks with the zero width and infinite amplitude. However, attributed to the mass operator, our theory can always yield peaks with a finite width and amplitude, because the mass operator has an imaginary part even for a real dielectric constant [in this case, we can evaluate the mass operator of Eq. (37) as the sum of a Cauchy principle value and the half residues from the poles of $1/\Delta(\lambda)$]. It should also be pointed out that the mode attenuation and hence the width of the enhanced peaks depends on the waveguide parameters. We will show how the mode attenuation changes with the waveguide thickness [see Fig. 4(b)]. Furthermore, since the mass operator has also a real part, the nulls of $Q(\lambda)$ would be different from the nulls of $\Delta(\lambda)$ [see Fig. 4(a)]. This means that the propagation constants of the guided modes are perturbed if the boundary of the waveguide is rough, as discussed in Sec. IV. Consequently, the locations of the satellite peaks will also be shifted from those given by the perturbation theory [the perturbed propagation constants are used to determine the locations of the peaks by Eq. (46) in our theory, while the unperturbed ones are used in the perturbation theory], although the shifts are very slight.

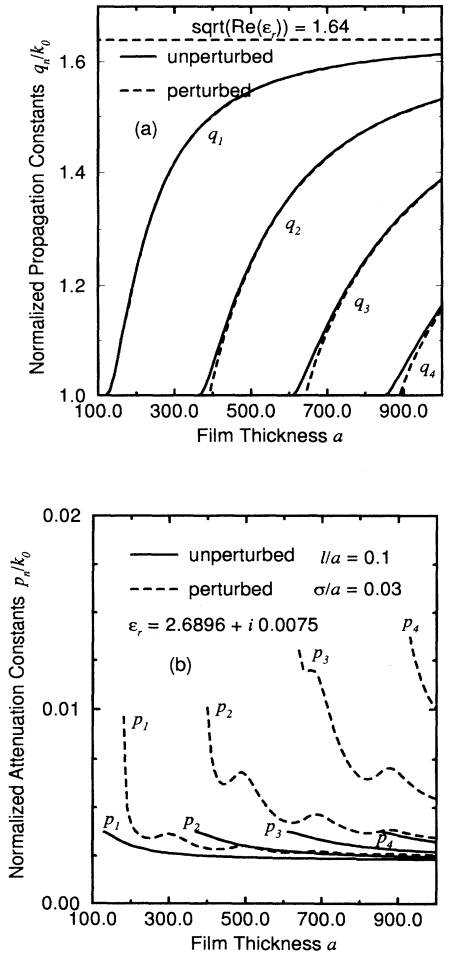

FIG. 4. Normalized propagation constants of the guided modes vs film thickness a. (a) The real part; (b) the imaginary part. The dielectric constant of the film is $\varepsilon_r = 2.6896 + i0.0075$. The wavelength is assumed to be 632.8 nm.

VI. NUMERICAL EXAMPLES AND DISCUSSIONS

For the purpose of numerical calculation we conveniently assume that the power spectrum of the random boundary has the Gaussian form

$$|F(\lambda)|^2 = \frac{\sigma^2 l}{\sqrt{\pi}} \exp(-\lambda^2 l^2) \ , \tag{51}$$

where σ and l are the parameters describing the roughness and the correlation length of the rough surface. The spectrum is a decreasing function of λ and has a maximum at $l = 1/\sqrt{2}\lambda$ as a function of l. From Eq. (11), the correlation function of the rough boundary is then given by

$$R(x) = \sigma^2 \exp(-x^2/4l^2) \ . \tag{52}$$

We note that the power spectrum used by us is related to that used in Ref. 25 by a factor $1/2\pi$, and the correlation length by a factor 2.

For convenience of the discussions below, we have shown in Fig. 4 the unperturbed and perturbed normalized propagation constants [Figs. 4(a) and 4(b) for the real and imaginary part, respectively] β_n/k_0 of the lowest and a few lower-order modes as a function of the film thickness a for the relative dielectric constant $\varepsilon_r = 2.6896 + i0.0075$ and the wavelength 632.8 nm. It can be seen that the ideal structure (no roughness) can support no guided mode as $a < 121.7$, one guided mode as $121.7 < a \leq 365.1$, two guided modes as $365.1 < a \leq 608.5$, three guided modes as $608.5 < a \leq 852.0$, and more than three guided modes as $a > 852.0$. The situation changes a little when the boundary of the waveguide becomes rough since the propagation constants are modified due to roughness. For the

slight rough boundary, the modifications on the real part are also slight as shown in the figure, except for the regions near the cutoff points of the modes, where the approximation Eq. (41) no longer retains its validity.[5,6] This means that the differences of the positions of the enhanced satellite peaks between our theory and the perturbation theory are very slight too. However, the modifications on the imaginary part (attenuation constant) are somewhat large, which means that the widths of the enhanced peaks should be evidently different from the perturbation theory by our theory.

We show in Figs. 5 and 6 the coherent scattering intensity $|A_0|^2$ as a function of the film thickness a and the incidence angle θ_0 for different values of the roughness parameters σ/a and l/a, respectively. The coherent scattering intensity behaves as an oscillating function of the thickness, even in the case of the absence of roughness. The effect of the roughness is just to make the oscillation deepen. Connecting the increase of the thickness to the appearance of the guided modes, we can conclude that the coherent scattering is much stronger in the neighbors where one of the guided modes begins to appear than in the regions where all of the guided modes are well guiding. In virtue of the energy conservation, we can expect that the incoherent scattering would be strong when the modes are well guiding, as shown below. The reason for this may be that in this case the modes can more actively interact with the rough boundary and provide more contributions to the radiation outside the waveguide. In the same way, we expect that the incoherent scattering becomes large as σ/a and l/a increase as well as when the incidence angle θ_0 is around 30°.

We compare in Fig. 7 the incoherent scattering distri-

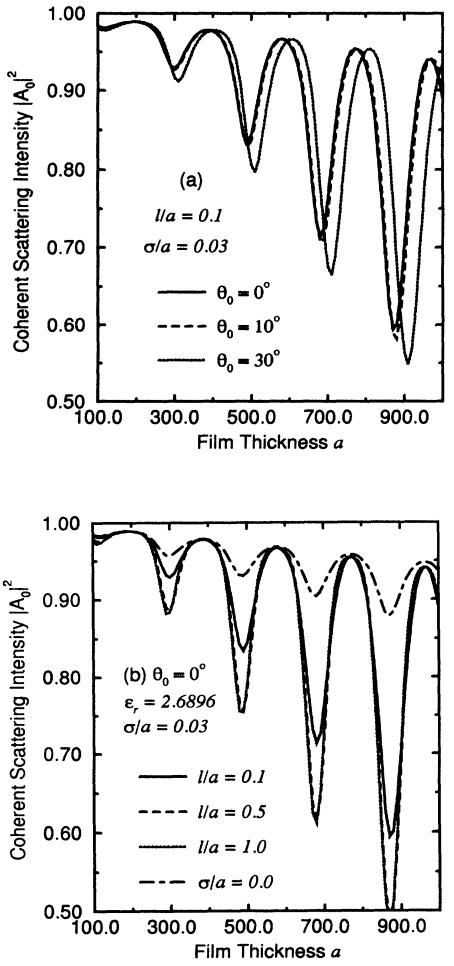

FIG. 5. Coherent scattering intensity $|A_0|^2$ vs film mean thickness a for different values of (a) the incidence angle $\theta_0=0°$, 10°, and 30° as $l/a=0.1$, and (b) the normalized correlation length $l/a=0.1$, 0.5, and 1.0 as $\theta_0=0°$. The normalized deviation of the rough surface is $\sigma/a=0.03$. The dielectric constant of the film is $\varepsilon_r=2.6896+i0.0075$. A plane wave with wavelength 632.8 nm is normal incident on the rough surface.

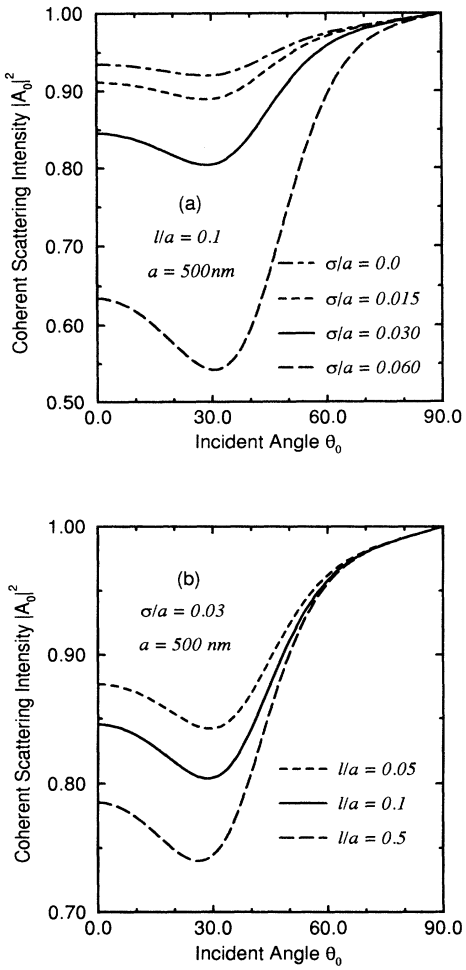

FIG. 6. Coherent scattering intensity $|A_0|^2$ vs incidence angle θ_0 for different values of (a) $\sigma/a=0.015$, 0.03, and 0.06 as $l/a=0.1$, and (b) $l/a=0.05$, 0.1, and 0.5 as $\sigma/a=0.03$. The mean thickness and the dielectric constant of the film are $a=500$ nm and $\varepsilon_r=2.6896+i0.0075$. The wavelength of the incident light is assumed to be 632.8 nm.

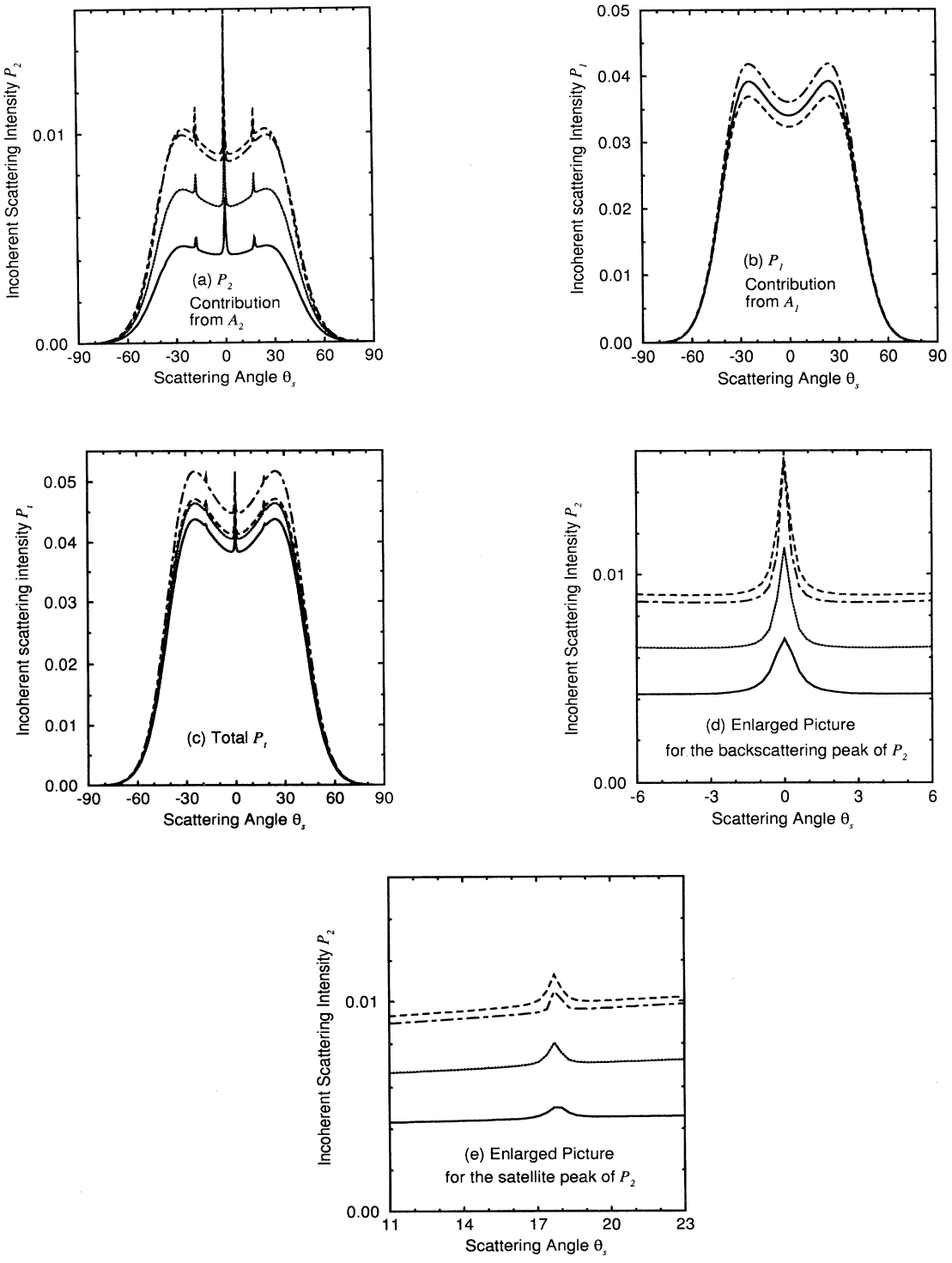

FIG. 7. Comparisons of the incoherent scattering distributions obtained by different calculations. The mean thickness and dielectric constant of the film are $a=500$ nm and $\varepsilon_r=2.6896+i0.0075$. The normalized parameters of the rough surface are $\sigma/a=0.03$ and $l/a=0.1$. The incident angle is $\theta_0=0°$ and the wavelength of the incident wave is assumed to be 632.8 nm. The contributions from the different orders of the Wiener kernels are plotted separately. (a) P_2, the contribution from the second-order kernel A_2; (b) P_1, the contribution from the first-order kernel A_1; (c) P_t, the sum of P_1 and P_2; (d) an enlarged picture of the part of (a) for the enhanced backscattering peak; and (e) an enlarged picture of the part of (a) for the enhanced satellite peak (on the positive side). The solid and dotted lines are, respectively, for the results obtained by our theory with and without the mass operator including in the integrand of P_2. The dashed line is for the results obtained by the perturbation theory. And the dot-dashed line is also for the results obtained by our theory with the mass operator inside the integrand of P_2 but is for $\varepsilon_r=2.6896$.

bution of our theory with that obtained by the perturbation theory for the parameters $a=500$ nm, $\varepsilon_r=2.6896+i0.0075$, $\sigma/a=0.03$, and $l/a=0.1$, when a plane wave of wavelength 632.8 nm is normal incident on the rough surface from outside the waveguide. The contributions arising from the first-order kernel A_1 and the second-order kernel A_2 are plotted separately. In addition to the well-known, strong, enhanced backscattering peak, two small satellite peaks symmetrically placed with respect to the backward direction $\theta_s=0°$ are also observed, and it is evident that the enhanced peaks originate entirely in the contribution P_2 from A_2. To demonstrate the effect of the mass operator on the enhanced peaks, we have shown in the same figure the results with and without the mass operator including in the integrand of P_2 [see Eq. (46)] for $\varepsilon_r=2.6896+i0.0075$, and also the results with the mass operator in for $\varepsilon_r=2.6896$. The integration for evaluating the mass operator is done directly for $\varepsilon_r=2.6896+i0.0075$, and with the help of the residue theorem and a principal value integration for $\varepsilon_r=2.6896$. For simplicity, only the values of the mass operator at the nulls of $\Delta(\lambda)$ are used at the neighbors of these nulls for the integration in P_2, based on the fact that the mass operator is not large enough to compare with $\Delta(\lambda)$, besides the neighbors of the nulls. Because we have already the mass operator in P_1 and in the outside of the integrand in P_2, it is not strange for us that our results are a little different from those of the perturbation theory, even without the mass operator inside the integrand of P_2. More importantly, we note that with the mass operator inside the integrand of P_2, the width of each enhanced peak is broadened and the amplitude decreases (arising from the imaginary part of the mass operator). The estimated values for the width of the enhanced peaks by Eq. (50) are 1.4° from the perturbation theory and 3.0° from our theory; these values roughly agree with those shown in Figs. 7(d) and 7(e). Moreover, as we mentioned in Sec. V, the locations of the peaks should be slightly shifted (arising from the real part of the mass operator), although we cannot observe the shifts easily in the figures because they are so slight. For instance, for the parameters given above, the locations of two peaks determined by the perturbation theory are $\theta_s=\pm 17.716°$, while they are $\theta_s=\pm 17.785°$ by our theory, so the shift is merely about 0.07° (it is only about 0.77°, even for $\sigma/a=0.1$). Furthermore, we have also shown that we can yield the enhanced peaks with the finite width and amplitude, even for a real dielectric constant, attributed to our mass operator.

Shown in Figs. 8–11 are the incoherent scattering distributions calculated by our theory without the mass operator inside the integrand of P_2, for the different values of the film thickness a and the number of the guided modes. As expected, there is just an enhanced backscattering peak when the structure can support only one mode, and other satellite peaks appear when the structure can support two or more modes. In principle, the number N of the satellite peaks relates to the number n of

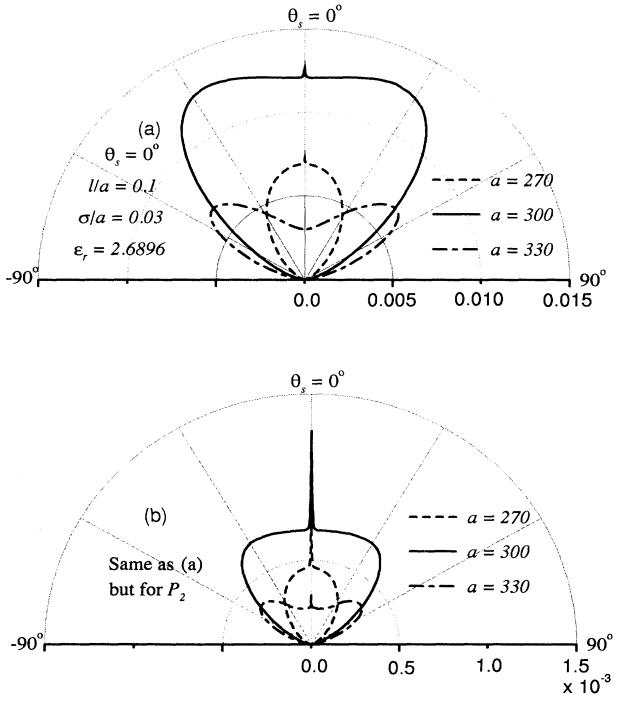

FIG. 8. Incoherent scattering distributions calculated with our theory without the mass operator inside the integrand of P_2 for different values of the mean thickness $a=270$, 300, and 330 nm, where the film structure can only support one guided mode. The roughness parameters are $\sigma/a=0.03$ and $l/a=0.1$, and the wavelength of the incident light is 632.8 nm. (a) The total P_t and (b) only P_2.

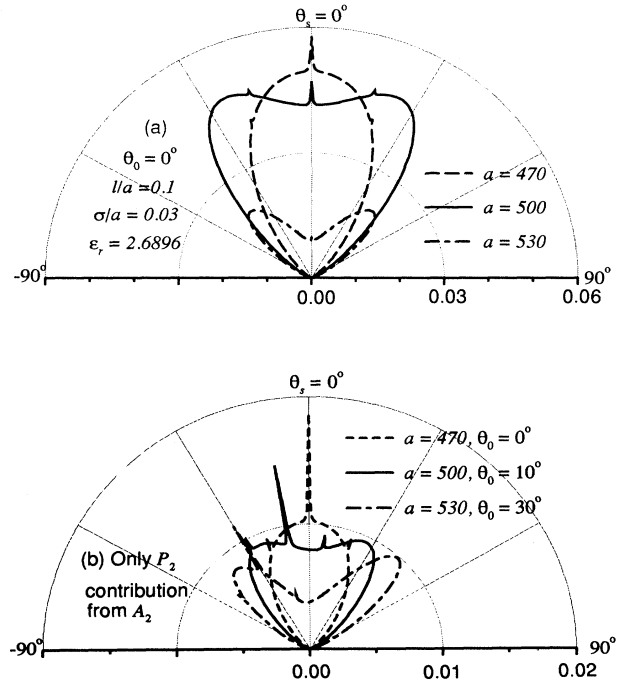

FIG. 9. Same as Fig. 8 but for different values of the mean thickness $a=470$, 500, and 530 nm, where the film structure can support two guided modes. (a) The total P_t and (b) only P_2.

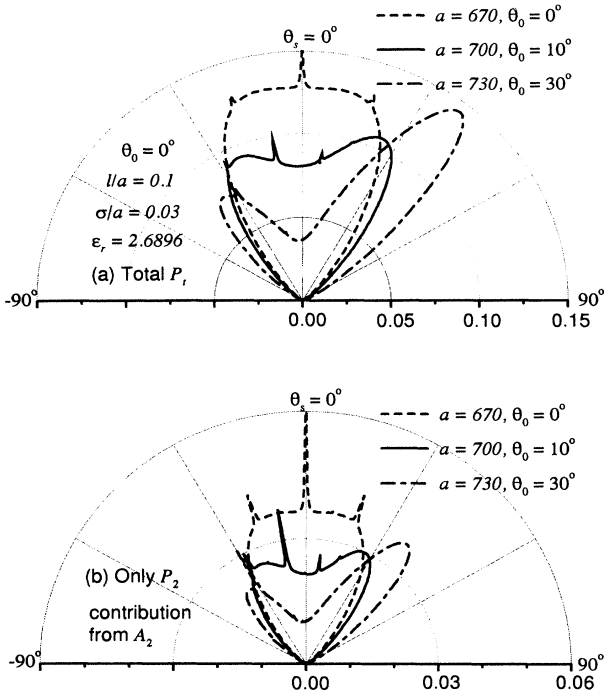

FIG. 10. Same as Fig. 8 but for different values of the mean thickness $a = 670$, 700, and 730 nm, where the film structure can support three guided modes. (a) The total P_t and (b) only P_2.

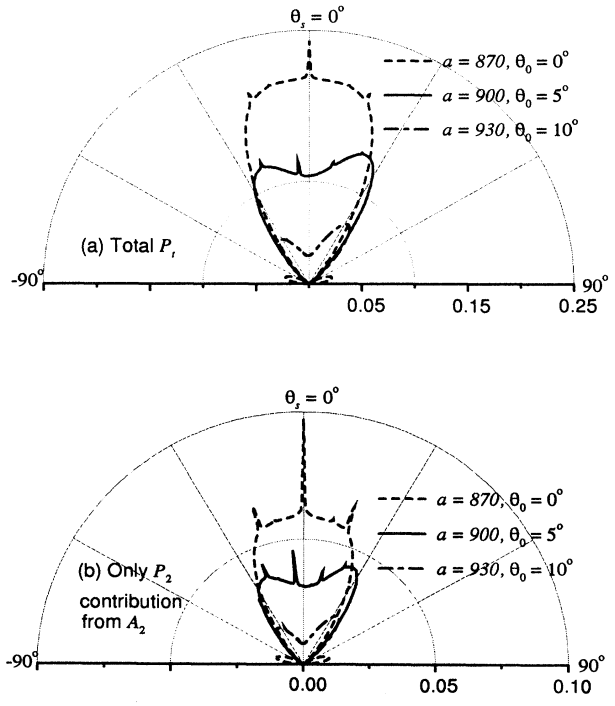

FIG. 11. Same as Fig. 8 but for different values of the mean thickness $a = 870$, 900, and 930 nm, where the film structure can support four guided modes. (a) The total P_t and (b) only P_2.

the modes by $N = n(n-1)$. For example, there should be six or twelve satellite peaks in the distributions if the structure can support three or four guided modes. However, we cannot observe so many peaks in Figs. 10 and 11. The reason may be due to the fact that certain interferences between the modes can cancel with each other and a few peaks drop into the angle regions where the incoherent scattering is very weak, leading to that some peaks are so small that they cannot be observed clearly. It is also noted that the shape and the strength of the incoherent distributions depend on the film thickness, or more precisely, the guiding state of the modes. And more importantly, the amplitudes of the enhanced peaks are also dependent on the guided state of the modes, but are not necessarily inversely proportional to the film thickness, contrary to their conjecture in Ref. 25.

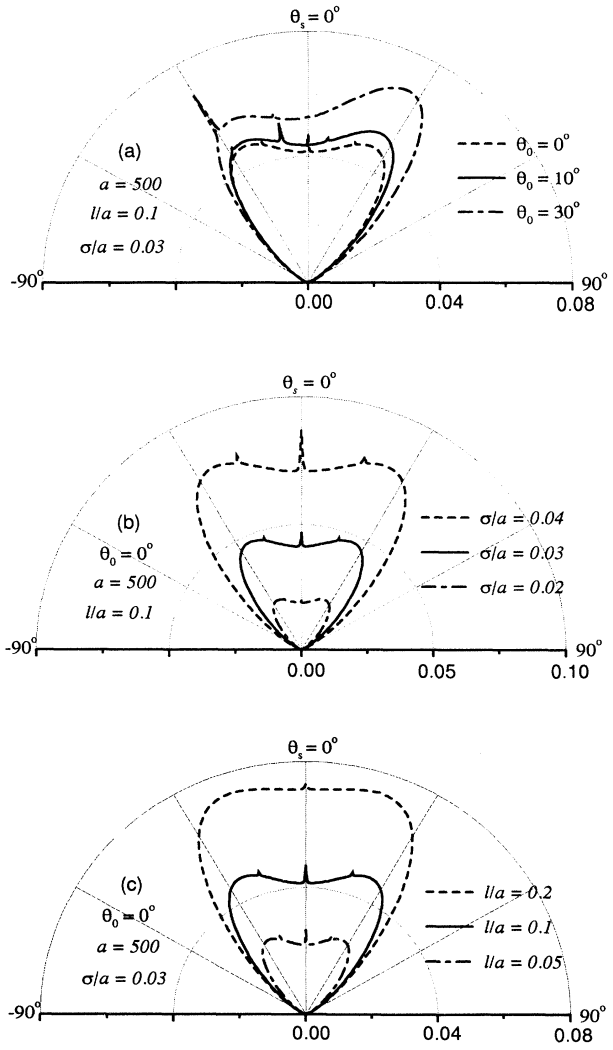

FIG. 12. Incoherent scattering distributions P_t calculated with our theory without the mass operator inside the integrand of P_2 for different values of (a) $\theta_0 = 0°$, 10°, and 30° as $\sigma/a = 0.03$ and $l/a = 0.1$, (b) $\sigma/a = 0.02$, 0.03, and 0.04 as $\theta_0 = 0°$ and $l/a = 0.1$, as well as (c) $l/a = 0.05$, 0.1, and 0.2 as $\theta_0 = 0°$ and $\sigma/a = 0.03$.

Figure 12 shows the incoherent scattering distribution for different values of the incidence angle θ_0, the normalized deviation σ/a, and the normalized correlation length l/a. The incoherent scattering becomes stronger as σ/a and l/a increase and θ_0 is around 30°, as we expected according to coherent scattering. However, it should be noted that the enhanced peaks no longer become stronger, but rather smaller after l/a arrived at a certain value. This is because, with the increase of l/a, the slope of the rough boundary also increases, and hence the radiations, contributed by the guided modes and originated to the enhanced peaks, is weakened by the shadow effect.

VII. CONCLUSIONS

In conclusion, we have treated the scattering problem of an *s*-polarized electromagnetic wave from a planar dielectric waveguide with one of its boundaries being a slightly rough surface and the other deposited on a perfectly conducting substrate, by applying the stochastic functional approach. Our theory is distinct from the common perturbation theory by the so-called mass operator, which contains much information about the interaction of the guided modes in the waveguide with the rough boundary and is very useful not only theoretically but also in numerical calculations. The numerical examples show that there are some satellite enhanced peaks in the incoherent scattering distribution, in addition to the well-known enhanced backscattering peak, if the structure can support two or more guided modes. In our terminology, these peaks originate by the interferences of two "double-scattering" processes described by the second-order Wiener kernel, in which the guided modes play the role of intermediate states. Since this kind of interference does not, after all, strongly take place for the various parameters, such enhanced peaks cannot be well observed unless certain conditions are satisfied.

ACKNOWLEDGMENT

One of the authors (Z.L.W.) would like to express his deep gratitude to International Communication Foundation of Japan (KDD's ICF) for its financial support of his visit in Japan.

---

*On leave from the National Key Laboratory of Optical Fiber Communications, University of Electronic Science and Technology of China, Chengdu 610054, People's Republic of China.

[1]P. Beckmann and A. Spizzichino, *The Scattering of Electromagnetic Waves from Rough Surfaces* (Pergamon, New York, 1963).

[2]F. G. Bass and I. M. Fuks, *Wave Scattering from Statistically Rough Surfaces* (Pergamon, Oxford, 1979).

[3]J. A. Ogilvy, *Theory of Wave Scattering from Random Rough Surfaces* (Hilger, Bristol, 1991).

[4]A. G. Voronovich, *Wave Scattering at Rough Surface* (Springer, Berlin, 1994).

[5]H. Ogura and Z. L. Wang, Phys. Rev. E **50**, 5006 (1994).

[6]Z. L. Wang, H. Ogura, and N. Takahashi, J. Opt. Soc. Am. A (to be published).

[7]H. Ogura, Phys. Rev. A **11**, 942 (1975).

[8]H. Ogura and J. Nakayama, Phys. Rev. A **11**, 957 (1975).

[9]H. Ogura and Y. Yoshida, Phys. Rev. A **14**, 796 (1976).

[10]J. Nakayama, H. Ogura, and B. Matsumoto, Radio Sci. **15**, 1049 (1980).

[11]J. Nakayama, H. Ogura, and M. Sakata, Radio Sci. **16**, 831 (1981).

[12]J. Nakayama, Radio Sci. **17**, 558 (1982).

[13]J. Nakayama, K. Mitzutani, and H. Ogura, J. Appl. Phys. **56**, 1465 (1984).

[14]H. Ogura and N. Takahashi, J. Opt. Soc. Am. A **2**, 2208 (1985).

[15]J. Nakayama, Radio Sci. **21**, 707 (1986).

[16]H. Ogura and J. Nakayama, J. Math. Phys. **29**, 851 (1988).

[17]H. Ogura, N. Takahashi, and M. Kuwahara, Wave Motion **14**, 273 (1991).

[18]H. Ogura, N. Takahashi, and M. Kuwahara, Waves in Random Media **1**, 363 (1991).

[19]H. Ogura, N. Takahashi, and M. Kuwahara, J. Math. Phys. **31**, 61 (1990).

[20]H. Ogura and N. Takahashi, in *Modern Techniques in Electromagnetic Theory,* edited by M. Tateiba and L. Tsang, Progress in Electromagnetics Research Vol. 11 (Elsevier, New York, 1995).

[21]K. Ito, Jpn. J. Math. **22**, 63 (1952).

[22]N. Wiener, *Nonlinear Problems in Random Theory* (MIT, Cambridge, MA, 1958).

[23]A. R. McGurn, A. A. Maradudin, and V. Celli, Phys. Rev. B **31**, 4866 (1985).

[24]J. Q. Lu, A. A. Maradudin, and T. Michel, J. Opt. Soc. Am. B **8**, 311 (1991).

[25]J. A. Sanchez-Gil, A. A. Maradudin, J. Q. Lu, V. D. Freulicher, M. Pustilnik, and I. Yurkevich, Phys. Rev. B **50**, 15 353 (1994).

[26]R. E. Collin, *Field Theory of Guided Waves,* 2nd ed. (IEEE, New York, 1991), Chap. 7.

[27]H. Ogura, *Theory of Stochastic Process* (Corona, Tokyo, 1978) (in Japanese).

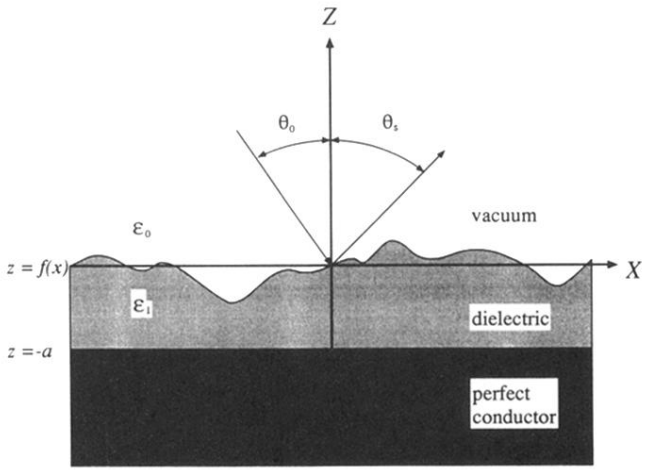

FIG. 1. The scattering structure studied in this work.